Effects of Glycosylation on the Structure and Dynamics of Eel Calcitonin in Micelles and Lipid Bilayers Determined by Nuclear Magnetic Resonance Spectroscopy[†,‡]

Yasuhiro Hashimoto,*[,§] Kazunori Toma,[‖] Joji Nishikido,[‖] Keizo Yamamoto,[‖] Katsuji Haneda,[‖] Toshiyuki Inazu,[‖] Kathleen G. Valentine,[⊥] and Stanley J. Opella[⊥]

Analytical Research Laboratory, Asahi Chemical Industry Company, Ltd., Fuji, Shizuoka 416-8501, Japan, The Noguchi Institute, Itabashi, Tokyo 173-0003, Japan, and Department of Chemistry, University of Pennsylvania, Philadelphia, Pennsylvania 19104

Received December 22, 1998; Revised Manuscript Received April 26, 1999

ABSTRACT: The three-dimensional structures of eel calcitonin (CT) and two glycosylated CT derivatives, [Asn(GlcNAc)3]-CT (CT-GlcNAc) and [Asn(Man_6-$GlcNAc_2$)3]-CT (CT-M6), in micelles were determined by solution NMR spectroscopy. The topologies of these peptides associated with oriented lipid bilayers were determined with solid-state NMR. All of the peptides were found to have an identical conformation in micelles characterized by an amphipathic α-helix consisting of residues Ser5 through Leu19 followed by an unstructured region at the C-terminus. The overall conformation of the peptide moiety was not affected by the glycosylation. Nevertheless, comparison of the relative exchange rates of the Leu12 amide proton might suggest the possibility that fluctuations of the α-helix are reduced by glycosylation. The presence of NOEs between the carbohydrate and the peptide moieties of CT-GlcNAc and CT-M6 and the amide proton chemical shift data suggested that the carbohydrate interacted with the peptide, and this might account for the conformational stabilization of the α-helix. Both the unmodified CT and the glycosylated CT were found to have orientations with their helix axes parallel to the plane of the lipid bilayers by solid-state NMR spectroscopy.

Glycopeptides are involved in a variety of important biological functions, where the carbohydrate moieties are essential for specific activities (*1*, *2*). Further, there are indications that the carbohydrate moiety is involved in the folding and stabilization of the three-dimensional structure of polypeptides. The structures and dynamics of several glycosylated proteins have already been elucidated by NMR or X-ray studies. While some of these studies have shown that the three-dimensional structures of the peptide moieties are not affected by the presence of the carbohydrate, in several notable cases the peptide conformation has been shown to be stabilized and its fluctuations restricted by the glycosylation (*3*−*9*). At present, however, there is little knowledge on the mechanism of how carbohydrates contribute to the stabilization of peptide conformation.

The newly developed chemoenzymatical synthesis method has made it possible to modify peptides with carbohydrates (*10*−*12*). By applying this method not only could the peptide derivatives with potent biological activities be developed, but also the functions of carbohydrates in glycopeptides could be clarified. We have already synthesized glycosylated calcitonin (CT)[1] and reported preliminary results about biological activity changes by the glycosylation (*13*−*16*). In such studies, it is also necessary to understand the structural and dynamical consequences by the carbohydrate substitution on the polypeptide.

This article compares the structures of the unmodified and the synthesized glycosylated eel CT derivatives: [Asn-(GlcNAc)3]-CT (CT-GlcNAc) and [Asn(Man_6-$GlcNAc_2$)3]-CT (CT-M6). Eel CT is a calcium-regulating peptide hormone composed of 32 amino acid residues and is not naturally glycosylated. The three-dimensional structures of several CTs, including those of human and salmon origin, have been elucidated by several groups using NMR (*17*−*22*) or circular dicroism (*23*, *24*). The common structural feature in the examples is the amphipathic α-helix. Since

[†] This work was performed as a part of the Research and Development Projects of Industrial Science and Technology Frontier Program and Joint Research supported by NEDO (New Energy and Industrial Technology Development Organization). This research utilized the Resource for Solid-State NMR of Proteins at the University of Pennsylvania, supported by Grant P41RR09731 from the Biomedical Research Technology Program, Division of Research Resources, National Institutes of Health.

[‡] The structural information has been deposited in the Brookhaven Protein Data Bank (filenames: 1bku, 1byv, 1bzb) and the BioMagResBank (filenames: 4219, 4260, 4261).

* Corresponding author. Present address: Department of Biochemistry, University of Oxford, Oxford OX1 3QU, U.K.

[§] Asahi Chemical Industry Co., Ltd.

[‖] The Noguchi Institute.

[⊥] University of Pennsylvania.

[1] Abbreviations: CT, calcitonin; GlcNAc, *N*-acetyl-D-glucosamine; Man, mannose; SDS, sodium dodecyl sulfate; HFIP, hexafluoro-2-propanol; NMR, nuclear magnetic resonance; NOESY, nuclear Overhauser effect spectroscopy; DQF-COSY, double-quantum-filtered shift correlated spectroscopy; TOCSY, total correlation spectroscopy; PISEMA, polarization inversion with spin exchange at the magic angle; DG, distance geometry; SA, simulated annealing; rmsd, root-mean-square deviation.

10.1021/bi983018j CCC: $18.00
Published on Web 06/06/1999

calcium regulation is thought to couple with membrane-bound receptor proteins (*25*, *26*), the amphipathic structural character of CT may play an important role in mediating interactions between peptide molecules and membrane-bound receptors. The proposed two independent binding sites in the receptor means that there is a possibility that different modes of peptide binding to the membrane may result in different interactions with the receptor and ultimately mechanisms of expression of biological activity (*22*). Thus, for further understanding of the function and the mechanism of calcitonin activity as well as the influence of the glycosylation, the topology of the peptide in the membrane is also an important issue.

The combination of solution and solid-state NMR analysis is a powerful method to determine structures of membrane-associated proteins. Proteins in micelles are studied by solution NMR spectroscopy to determine the high-resolution three-dimensional structure. Solid-state NMR spectroscopy of peptides in oriented phospholipid bilayers is capable of determining the overall topology of the peptide in the membrane. This method has been successfully applied to several membrane-associated peptides and proteins (*27*−*33*).

Our investigation of the unmodified and the glycosylated eel CT addresses the conformational changes and the stabilization of the peptide by the glycosylation, the orientation of the sugar moiety relative to the peptide in micelles, and the topology of the peptide molecule associated with lipid bilayers.

MATERIALS AND METHODS

Sample Preparation. Eel CT was purchased from Bachem California. CT-GlcNAc was synthesized by Boc strategy in solid phase using N^{α}-(*tert*-butyloxycabonyl)-N^{ω}-(2-acetamido-2-deoxy-α-D-glucopyranosyl)-L-asparagine (Boc-Asn-(GlcNAc)) (*13*). CT-M6 was prepared using chemoenzymatic synthetic methods (*12*), where Man_6-GlcNAc moiety was transglycosylated to CT-GlcNAc by *endo-β-N*-acetylglucosaminidase (*14*, *15*). The purity of each sample was checked by reverse-phase HPLC monitoring UV absorption at 214 nm. CT-GlcNAc contains *N*-acetyl-D-glucosamine (GlcNAc) attached to the Asn3 residue of calcitonin. CT-M6 contains N-linked high-mannose-type oligosaccharide, M6, binding at Asn3. The chemical structures of these are shown in Figure 1.

Solution NMR. The calcitonin samples were dissolved in 0.22 mL of H_2O/D_2O = 9/1 containing 0.05 M CD_3COOD, together with sodium dodecyl sulfate (SDS)-d_{25} at peptide/SDS molar ratio of 1:100.

All solution NMR spectra were obtained with a Bruker DMX 750 spectrometer. The series of two-dimensional NMR experiments, including DQF-COSY, TOCSY, and NOESY, used in the structural analysis was recorded at 308 K in the phase-sensitive mode using time proportional phase incrementation. In these experiments, the water signal was suppressed using a 2-s presaturation pulse during the recycle delay. A series of NOESY spectra was recorded with several mixing times: 100, 150, and 200 ms. TOCSY spectra were recorded with 40-, 60-, and 80-ms mixing times for magnetization transfer. The assignments of peptide resonances except for some protons of Pro32 (CT) or Thr31 and Pro32 (CT-GlcNAc, CT-M6) were achieved using the sequence-specific resonance assignment methods introduced by Wüthrich et al. (*34*). In cases where there was spectral overlap with H_2O, spectra were also recorded at 338 K. For glycosylated CTs, however, we obtained assignments for only about half the protons of the carbohydrate moiety due to resonance overlap.

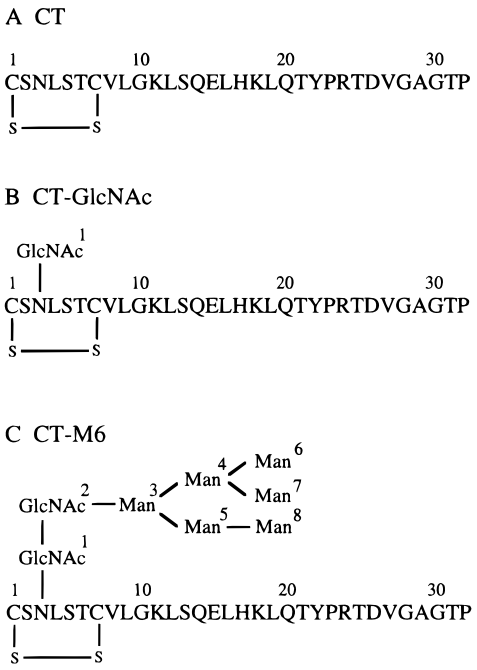

FIGURE 1: Chemical structures of CT, CT-GlcNAc, and CT-M6.

NMR-Derived Constraints. Nuclear Overhauser effect (NOE) distance constraints were obtained from NOESY data using the FELIX programs (Molecular Simulation Inc.). The strong, medium, and weak NOEs observed in the experiments with 150-ms mixing time were grouped into three distance ranges: 1.8−2.9, 1.8−3.8, and 1.8−5.0 Å, respectively. A total of 184 NOEs for CT, 183 NOEs (intra-polypeptide, 178; polypeptide-carbohydrate, 5) for CT-GlcNAc, and 185 NOEs (intra-polypeptide, 175; polypeptide-carbohydrate, 5; inter-carbohydrate residue, 5) for CT-M6 were used as constraints for distance geometry calculations. Additionally, hydrogen bonds identified on the basis of slowly exchanging amide protons were incorporated as distance constraints with 1.8 Å < d_{H-O} < 2.2 Å and 2.8 Å < d_{N-O} < 3.3 Å. These hydrogen bond constraints were applied only for the pairs of residues where helical NOEs, $d_{\alpha N}(i,i+3)$ and $d_{\alpha\beta}(i,i+3)$, were apparently observed. The hydrogen-bonding pairs were also confirmed by checking structures calculated using only NOEs.

Distance Geometry and Simulated Annealing Calculations. Structure calculations were performed with NMRchitect (Molecular Simulation Inc.) using the distance geometry/simulated annealing (DG/SA) protocol. In the calculations for the glycosylated CT, the carbohydrate residues were fixed in the boat form. The calculations were started from 20 randomized structures. On the basis of the number of constraint violations and the energy values, the 10 best structures were selected and statistics compiled from these structures.

Solid-State NMR Spectroscopy. For the solid-state NMR studies, specifically [^{15}N]Leu12-labeled CT, CT-GlcNAc and CT-M6 were synthesized using ^{15}N-labeled Leu in a similar

manner as described in the sample preparation. Membrane-bound samples were prepared as follows: 2−4 mg of each peptide was mixed with palmitoyl-oleoyl-phospatidylcholine (POPC) (80%) and palmitoyl-oleoyl-phospatidylglycerol (POPG) (20%) at approximately 1 mol % peptide in the lipids. The peptide and lipids were then dissolved in chloroform containing trace amounts of H_2O and hexafluoro-2-propanol (HFIP) and spread onto 25 thin glass plates (11 × 11 × 0.05 mm). After air-drying, the glass plates were stacked and placed in a sealed chamber for 12−24 h together with a saturated ammonium phosphate solution which provided a 94% relative humidity atmosphere. The sample was sealed with plastic film before insertion into the coil of the NMR probe.

All solid-state NMR spectra were obtained with a home-built 700-MHz NMR spectrometer. For the one-dimensional ^{15}N chemical shift NMR spectra, 256 data points were acquired using cross-polarization at a field strength of 52 kHz with a mixing time of 1 ms and high-power proton decoupling at a field strength of 62 kHz during the data acquisition time and the recycle delay of 8 s. Two-dimensional $^{1}H-^{15}N$ dipolar coupling/^{15}N chemical shift PISEMA spectra (*33*) were measured with 700 (CT) or 1400 (CT-GlcNAc, CT-M6) transients for each of 16 (CT-GlcNAc) or 32 (CT, CT-M6) t_1 increments. The mixing time for cross-polarization was 1 ms, and the recycle delay was 8 s. The data were processed using the FELIX program.

RESULTS

Three-Dimensional Structure Determination of Unmodified CT in Micelles. The intra- and interresidue NOEs were assigned starting from the peptide resonance assignments. The NOE pattern of CT is summarized in Figure 2A, together with the deuterium-exchange rates of the amide protons and the chemical shift indices. In the region of Leu4−Tyr22, $d_{\alpha N}(i,i+3)$ and $d_{\alpha\beta}(i,i+3)$ NOEs were observed, which is characteristic for an α-helix conformation. The existence of the α-helix was also indicated by successive d_{NN} connectivities in this region and the slower amide proton exchange observed in the region of Ser5−Leu19 except for His17. Slowly exchanging protons are generally regarded as involved in hydrogen bonding as those protons are unlikely to be buried in the interior of a biomolecule as small as CT. Further the negative values of the chemical shift indices support the presence of an α-helix in this region.

The C-terminal region of the peptide, Pro23−Pro32, showed no medium or long-range interresidue NOEs. Also, in this region, the chemical shifts were mostly identical to those of the random coil (*34*). Therefore, the C-terminal 10 residues are considered to be a random structure.

The structure calculation of CT was performed by incorporation of the NOE data and the deuterium-exchange data into the DG/SA protocol. From the 20 calculated structures, 10 were selected based on the energy value and the number of constraint violations. The superposition of the 10 structures is shown in Figure 3. As expected from the NOE connectivities, CT is mainly characterized by an α-helix in Ser5−Leu19 and it frays open at the region of Gln20−Tyr22 followed by a random coil structure. The N-terminal residues form a looplike structure to accommodate the disulfide bridge between Cys1 and Cys7. Although in the region of Gln20−Tyr22 the NOE patterns typical for an α-helix were observed as mentioned above, the amide protons in these residues showed rapid exchange with deuterium. Also the intensities of the α-helical NOEs of this part were weaker compared with those observed in the α-helix region. From this observation we propose that the residues of Gln20−Tyr22 retaining a helical character adopt a somewhat fluctuating conformational intermediate between the random structure and the α-helix. As for the N-terminal end of the helix, the observation of a $d_{\alpha\beta}(i,i+3)$ NOE from Leu4 to Cys7 suggests that the helix termination may include Leu4. However, the backbone dihedral angles of the calculated structures start spreading from the residues of Ser5 and Leu4. Thus we assigned the range of the helix from Ser5 to Leu19. The rmsd among the backbone atoms of the helical stretch of the CT peptide was 0.51 Å for the best 10 structures.

Three-Dimensional Structure Determination of CT-GlcNAc in Micelles. The NOE connectivities, chemical shift indices, and exchange data for CT-GlcNAc are shown in Figure 2B. Some NOEs, $d_{\alpha N}(i,i+3)$ and $d_{\alpha\beta}(i,i+3)$, characteristic for an α-helix were overlapped in the two-dimensional spectrum and thus were omitted from Figure 2B. This results in the smaller number of NOEs for the α-helix than for unmodified CT. However, the pattern of NOEs of CT-GlcNAc as well as the slow exchange amide protons is identical to those of unmodified CT. Further, the negative chemical shift values up to Thr21 and those corresponding to the random coil in the C-terminal region of the peptide show the same trend observed in unmodified CT.

In the calculated structures shown in Figure 3, the CT-GlcNAc has the same features as unmodified CT, an α-helix in Ser5−Leu19 with a random coil conformation at the C-terminus. Between them comes a somewhat disordered intermediate structure (Gln20−Tyr22). In the N-terminus, looplike conformation through the disulfide bridge between Cys1 and Cys7 occurs. The rmsd of the helical stretch among the backbone atoms for the best 10 structures is 0.45 Å. Thus, there is no apparent difference between the structures of CT and CT-GlcNAc, indicating that the overall conformation of the peptide structure is not influenced by the GlcNAc residue.

Three-Dimensional Structure Determination of CT-M6 in Micelles. Although as is the case for CT-GlcNAc, some NOEs characteristic for a helical structure were overlapped with other signals, the same structure components in the identical region with CT and CT-GlcNAc, the α-helix region, the random coil structure in the C-terminus, and the looplike structure in the N-terminal region were indicated by the NOE pattern, slow exchange amide protons, and chemical shift indices (Figure 2C). The calculated structures (Figure 3) show the same conformational feature as CT and CT-GlcNAc. And as observed in CT and CT-GlcNAc, Gln20−Tyr22 residues, leading to the α-helix, have somewhat spreading conformation compared with those in the helix region. The degree of spreading was the same in all three samples. Thus, CT-M6 was revealed that, though containing the M6 oligosaccharide of such a large molecular size, the peptide moiety has the identical overall conformation with CT and CT-GlcNAc. The rmsd among the backbone atoms of the helical stretch of the peptide moiety was 0.55 Å for the best 10 structures.

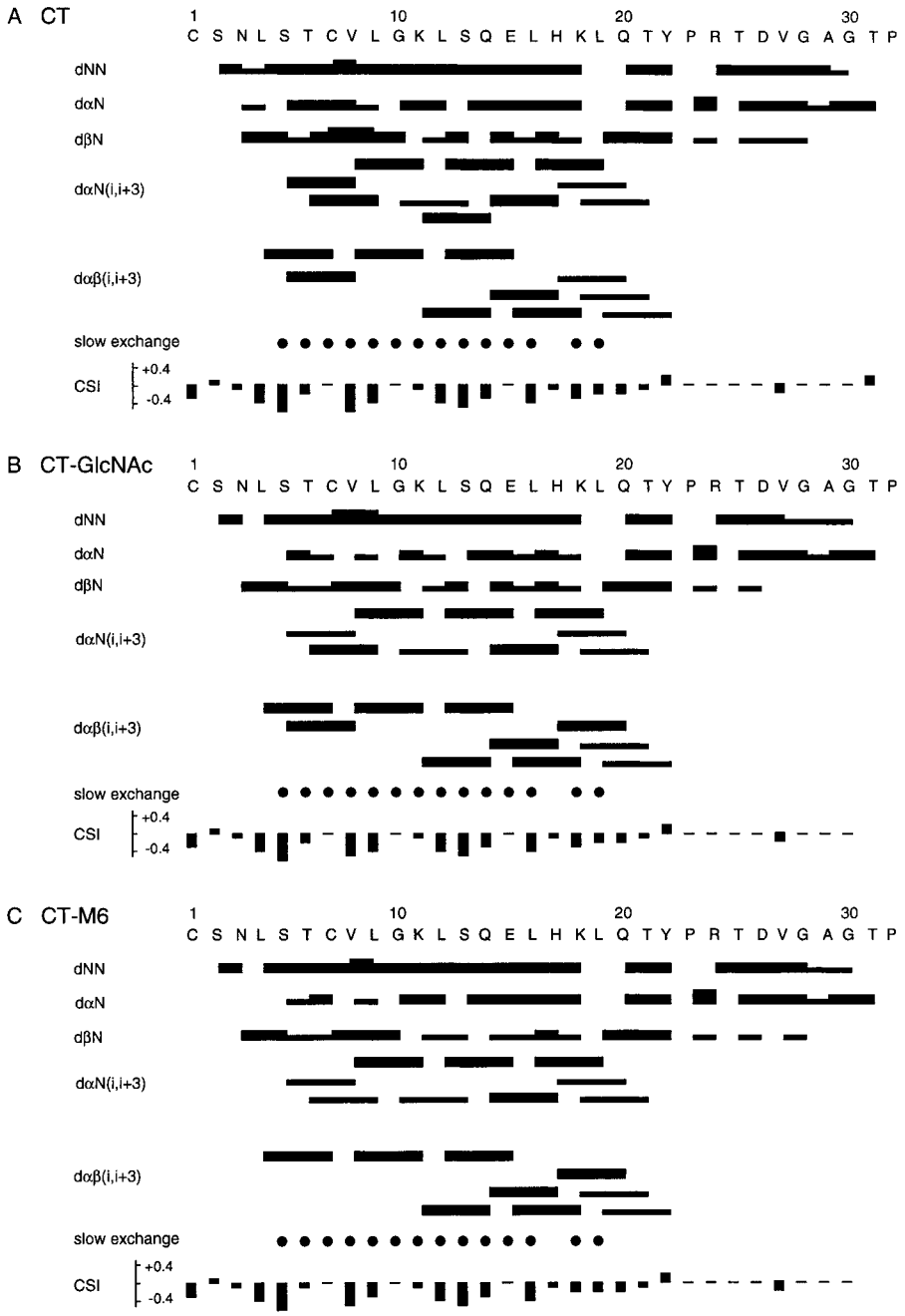

FIGURE 2: Summary of NOEs, CαH chemical shift index, and NH exchange data of CT, CT-GlcNAc, and CT-M6. NOE intensities are indicated by the height of the bars. Ambiguous NOEs due to resonance overlaps are omitted from the maps. Circles indicate slow exchange NH protons which were still visible after 6 h in D_2O.

Orientation of the Sugar Moiety in Micelles. NOEs were observed between the carbohydrate and the peptide moieties in CT-GlcNAc. As shown in Figure 4, GlcNAc1 protons (H1, -2, -3, -5) had NOEs with the Thr6 methyl protons, which are located near the beginning of the α-helix. Since the H4 and H6 proton chemical shifts could not be assigned, the NOEs from these protons were unclear. From these observed NOEs as well as the calculated structures, the GlcNAc1 moiety was found to have a somewhat restricted conformation that interacted with the N-terminal portion of the α-helix. Also, chemical shift data may suggest this interaction. Figure 5 shows the chemical shift differences between the three samples. The large chemical shift changes of the amide hydrogen resonances around Ser2−Val8 in CT-GlcNAc (Figure 5A) were likely the result of interactions between the carbohydrate and the peptide moieties. A detailed analysis of the calculated structures of CT-GlcNAc suggested that the GlcNAc1 residue could adopt two possible conformations that are consistent with the NOE data. As depicted in Figure 6, in conformation A the H1, H3, and H5 protons were close to the Thr6 methyl group, while in conformation B, only the H2 was close to the Thr6 methyl protons.

CT-M6 also has the similar pattern of NOEs to that observed for CT-GlcNAc (Figure 4), and in the calculated structures two conformations A and B (Figure 6) of GlcNAc1 in the M6 moiety were observed. No additional NOEs arising from the interaction between the peptide and the carbohydrate groups were observed. Although NOE data showed that only the GlcNAc1 residue in the M6 moiety had interactions with the peptide moiety, we obtained the chemical shift data

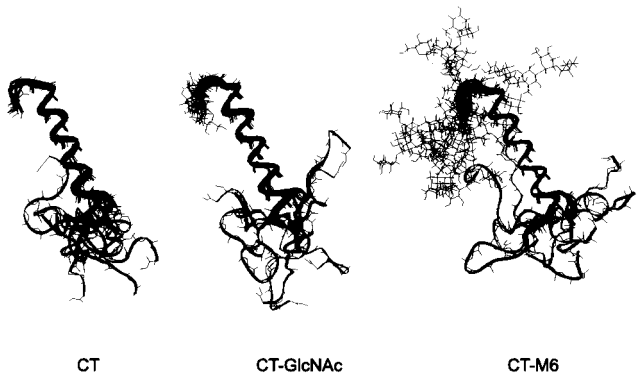

FIGURE 3: Three-dimensional structures of CT, CT-GlcNAc, and CT-M6 in SDS micelles shown as a superposition of the backbone atoms of the 10 lowest energy structures. The structures are aligned at residues 5−19.

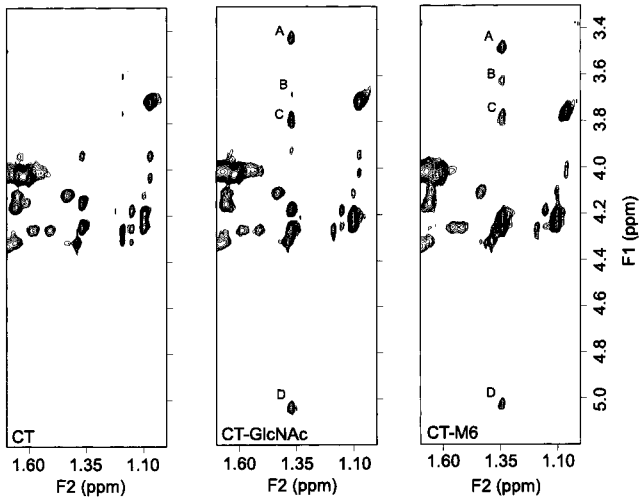

FIGURE 4: NOEs between the GlcNAc1 residue protons and the Thr6 methyl protons in NOESY spectra with 150-ms mixing time. NOE peaks are assigned to (A) Thr6 CH_3−GlcNAc1 H5; (B) Thr6 CH_3−GlcNAc1 H3; (C) Thr6 CH_3−GlcNAc1 H2; (D) Thr6 CH_3−GlcNAc1 H1.

(Figure 5B) that could be evidence for interactions between the central region of the α-helix and the sugar moiety. While CT-GlcNAc showed large chemical shift changes of the amide protons at the N-terminus up to Val8, the M6 structure influenced the chemical shifts as far as the Gln14 residue. The lack of NOEs between M6 and the helix except for the GlcNAc1 residue, however, suggests that the interaction of the M6 moiety and the helix is weak and transitory.

Orientation of α-Helices of CT, CT-GlcNAc, and CT-M6 in Lipid Bilayers. To obtain information on how CT interacts with membranes and whether the glycosylation affects it, solid-state NMR experiments were performed on the unmodified and the glycosylated CTs in oriented phospholipid bilayers. In these experiments, ^{15}N chemical shift as well as $^{15}N-^{1}H$ dipolar coupling frequency provides angular constraints on the orientation of the helix axis relative to the plane of the lipid bilayers (*35*−*38*). When the sample is arranged so that the glass plates, which correspond to the lipid bilayer plane, are orthogonal to the direction of the applied magnetic field, the ^{15}N chemical shift of 70−80 ppm ($\sigma_\perp$) and the approximately 10 kHz $^{15}N-^{1}H$ dipolar coupling constant indicate the presence of an in-plane helix orientation relative to the lipid bilayer. In contrast, an orientation of the

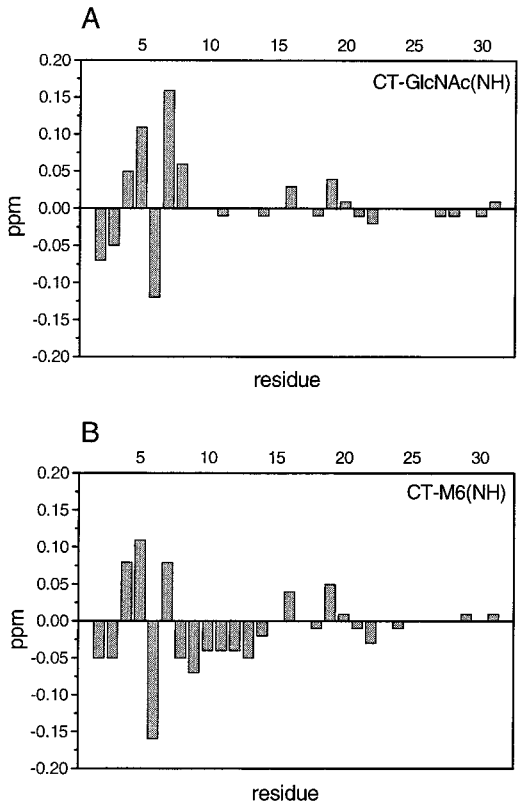

FIGURE 5: Comparison of the amide proton chemical shifts between CT, CT-GlcNAc, and CT-M6. The values of shift differences were obtained by subtracting the chemical shift value of CT from that of CT-GlcNAc or CT-M6, respectively.

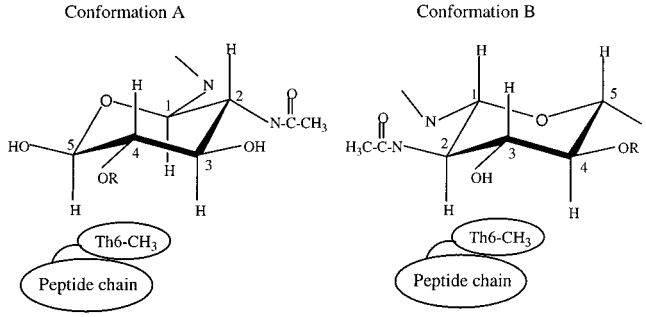

FIGURE 6: Schematic drawing of possible conformations of the GlcNAc1 residue. CT-GlcNAc, R = H; CT-M6, R = GlcNAc2. The rotation of Asn3 side chain could make these two different orientations.

helix perpendicular to the lipid bilayer would result in values of 210−220 ppm chemical shift ($\sigma_{||}$) and about 20 kHz $^{15}N-^{1}H$ dipolar coupling, and an unoriented helix shows a powder pattern. The one-dimensional ^{15}N chemical shift spectrum of [^{15}N]Leu12-CT together with a calculated powder pattern is shown in Figure 7A,D. A narrow single-line resonance was observed at 70 ppm. Although this resonance arises from the backbone amide nitrogen site of Leu12 alone, since Leu12 is situated in the center of the α-helix, this result can be considered to represent the orientation of the entire helix. The chemical shift indicates that the α-helix lies in the plane of the lipid bilayer. Furthermore, as is indicated in Figure 7B,C, both glycosylated peptides [^{15}N]Leu12-CT-GlcNAc and [^{15}N]Leu12-CT-M6 also had the same chemical shift values in their solid-state NMR spectra. The orientation of the peptide helices was confirmed by the two-dimensional

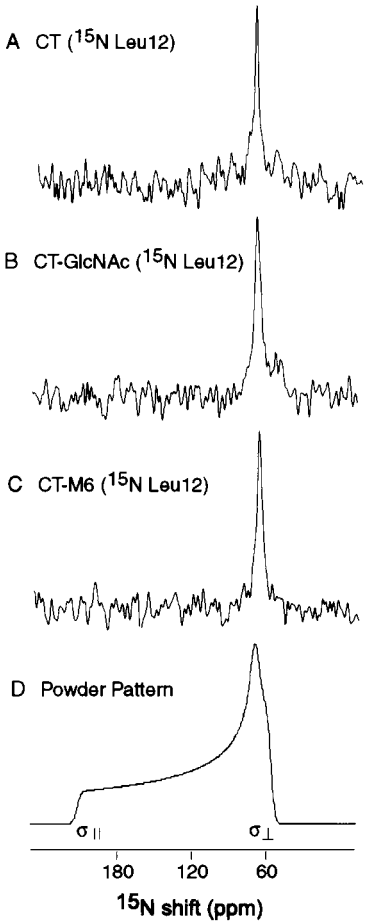

FIGURE 7: One-dimensional ^{15}N NMR spectra of selectively [^{15}N]-Leu12-labeled CT, CT-GlcNAc, and CT-M6 in oriented lipid bilayers. The chemical shifts of samples are 71.3 ppm (CT), 70.1 ppm (CT-GlcNAc), and 69.4 ppm (CT-M6). The experimental spectra are compared to a calculated ^{15}N amide chemical shift powder pattern with the positions of the principal elements marked.

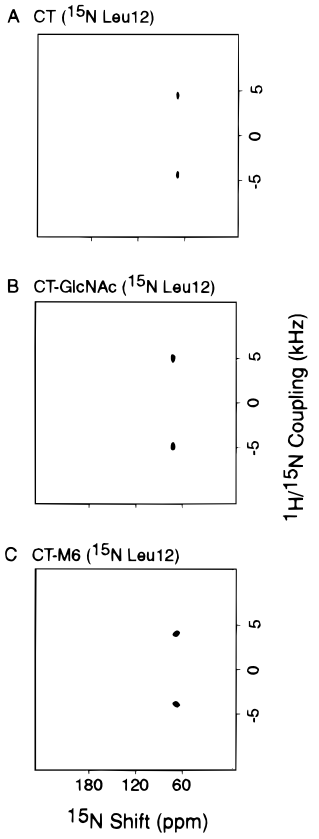

FIGURE 8: Two-dimensional ^{1}H−^{15}N dipolar coupling/^{15}N chemical shift PISEMA spectra of selectively [^{15}N]Leu12-labeled CT, CT-GlcNAc, and CT-M6 in oriented lipid bilayers. The dipolar coupling frequencies of samples are 9 kHz (CT), 10 kHz (CT-GlcNAc), and 8 kHz (CT-M6).

^{1}H−^{15}N dipolar coupling/^{15}N chemical shift PISEMA spectra. Figure 8 shows that both the unmodified and the glycosylated CTs had 8−10 kHz dipolar couplings corresponding to the value for an α-helix in plane relative to the lipid bilayer (CT, 9 kHz; CT-GlcNAc, 10 kHz; CT-M6, 8 kHz). The experimental dipolar coupling frequencies measured for the limited number of samples are similar and may be the same within the limitations of preparing separate samples, aligning the material on glass plates, and then aligning the plates in the coil of the spectrometer. The practical limit on determining the orientation of a helix in a bilayer with multiple single-site-labeled samples is likely to be about 10°, although the experiments and interpretations are fundamentally capable of higher structural resolution.

The combination of the ^{15}N chemical shift with the ^{15}N−^{1}H dipolar coupling data indicates that the peptide adopts an in-plane helical configuration and that the glycosylation does not alter the orientation of the peptide with respect to the lipid bilayers.

DISCUSSION

CT, CT-GlcNAc, and CT-M6 have essentially the same structure in SDS micelles, characterized by an α-helix followed by a random coil region at the C-terminus. The N-terminus has a looplike structure induced by the disulfide bond between residues Cys1 and Cys7. These structural features have already been reported for CTs of different species. The length of the α-helix varies according to the amino acid sequence and the sample solution (e.g., salmon CT in 90% methanol, Val8−Tyr22 (*18*); salmon CT in SDS, Thr6−Tyr22 (*20*); elcatonin in 40% trifluoroethanol, Thr6−Thr21 (*21*); human CT in SDS, Leu9−Phe16 (*22*)). The resemblance in the length of α-helices between salmon CT, elcatonin, and eel CT may result from their similarity of the amino acid sequences, while human CT having the lower sequence similarity results in the shorter helix. The conformation of the C-terminal region of CTs has been an issue. One example indicated that the peptide chain in the C-terminal region folds back toward the α-helix (*20*), while others indicated no association between them, showing an extended random coil structure in the C-terminus (*18*, *22*). However, as salmon CT showed different conformations in the C-terminus according to the sample solution, the solvent system can affect the conformation of CTs.

Elcatonin is a synthetic analogue of eel CT, and the disulfide bond is replaced by an ethylene bridge by substituting 7-aminosuberic acid for the 1 and 7 positions of eel CT. Comparison of elcatonin (*21*) and our results shows that both of the peptides retain similar features. However a difference is found in the length of the α-helix (elcatonin, Thr6−Thr21). Further, they suggest from the $d_{\alpha N}(i,i+2)$ NOE that a turn structure occurs in the segment of Arg24−Asp26, which is not found in our case. Again, we have to take into consideration the effect of the solvent system.

The comparison of the structures, unmodified and glycosylated CTs, indicates the overall conformation is not affected by the glycosylation, despite the large molecular size of the M6 moiety attaching to the peptide. Examples, in which three-dimensional structures of peptides are not affected by glycosylations, have been reported. For example, Mer and colleagues (*39*) have compared the structures of fucosylated and free PMP-C and found the conformational changes only in the vicinity of the fucose moiety. They, however, suggested that the fucosylation was responsible for an overall decrease of the dynamic fluctuations of the molecule from the amide proton-exchange experiments. Wyss et al. (*40*) proved that the N-linked high-mannose-type oligosaccharide in the adhesion domain of human CD2 adopted a well-defined conformation, in which mobility of the carbohydrate moiety was restricted. Further, they suggested that the carbohydrate stabilizes the protein fold.

We compared the amide proton-exchange rate between samples by two-dimensional NOESY spectra in D_2O solution and found that the glycosylated CTs showed a lower exchange rate at Leu12 than the unmodified CT (data not shown). We could not further investigate other residues in the α-helix due to the poor resolution of the spectra. However, this limited data may partly explain the dynamical behavior of the helix, since Leu12 is situated in the center of the helix, and as shown by O'Neil and Sykes (*41*) there is no influence of being buried in micelles on exchange rates and it could serve as monitors of hydrogen bonding and protein structure in micelles. Further, GlcNAc residue cannot span this length of the helix as can be seen in Figure 3, eliminating the possibility that the restricted exchange rate originated from limited accessibility of D_2O. Thus, the lower exchange rate of Leu12 amide proton proposes the possibility that the α-helix of CT be stabilized with its fluctuations restricted by the glycosylation.

The GlcNAc1 residues in both CT-GlcNAc and CT-M6 were indicated by NOEs to adopt a conformation close to the N-terminal end of the α-helix. The carbohydrate appears to cap the α-helix at the N-terminal end, and this may contribute to the stabilization of the helix. The stabilization of the α-helix and the hypothesis of the mechanism described above are important for the application of carbohydrates in the development of new materials; thus we will further investigate this point by varying the carbohydrate structure and its binding site.

Structure−activity studies of CTs of several species have demonstrated the importance of an amphipathic α-helix in the pharmacological activity (*23*), in which its amphipathic character promotes the molecular binding to the membrane or the receptor. Motta et al. pointed out a possibility that different topologies could be taken in bilayer by peptide having the similar secondary structure in micelles (*22*). This might lead to different mechanisms of interaction with the membrane, the receptor and, hence, the expression of the biological activity. They suggested two possible topologies of the α-helix in binding: (a) tangential interaction of the human CT amphipathic helix with the membrane surface and (b) perpendicular insertion into the membrane of the wedge-like helix−tail structure, similar to that of salmon CT. Our solid-state NMR experiments have shown that eel CT is associated with the lipid bilayers taking a helical conformation, and the helix axis of the peptide is in the plane of the bilayers. As the amino acid sequence and the biological activity of eel CT resemble those of salmon CT, we suspect the interaction with the membrane might also be the same for both CTs.

The comparison of the solid-state NMR data between the unmodified and glycosylated CTs revealed that the glycosylation does not affect the binding topology of the helix. The accumulation of this structural knowledge for CTs of various species as well as the influence of glycosylation will clarify the function and the mechanism of the CTs. Further, this will be applied to the design of new materials with higher activities, such as the ones modified with carbohydrates. At present we are continuing the investigation of the influence of glycosylation on the binding affinity of CT to the receptor and the biological activity of the molecules.

ACKNOWLEDGMENT

We thank Ms. Tagashira for assistance of structure calculations and also Prof. Kobayashi (Osaka University) and Mr. Ogawa for valuable comments for NMR studies.

REFERENCES

1. Recny, M. A., Luther, M. A., Knoppers, M. H., Neidhardt, E. A., Khandekar, S. S., Concino, M. F., Schimke, P. A., Francis, M. A., Moebius, U., Reinhold, B. B., Reinhold, V. N., and Reinherz, E. L. (1992) *J. Biol. Chem. 267*, 22428−22434.
2. Rudd, P. M., Joao, H. C., Coghill, E., Fiten, P., Saunders, M. R., Opdenakker, G., and Dwek, R. A. (1994) *Biochemistry 33*, 17−22.
3. Kessler, H., Matter, H., Gemmecker, G., Kottenhahn, M., and Bats, J. W. (1992) *J. Am. Chem. Soc. 114*, 4805−4818.
4. Shogren, R., Gerken, T. A., and Jentoft, N. (1989) *Biochemistry 28*, 5525−5536.
5. Gerken, T. A., Butenhof, K. J., and Shogren, R. (1989) *Biochemistry 28*, 5536−5543.
6. Shaanan, B., Lis, H., and Sharon, N. (1991) *Science 254*, 862−866.
7. Joao, H. C., Scragg, I. G., and Dwek, R. A. (1992) *FEBS Lett. 307*, 343−346.
8. Andreotti, A. H., and Kahne, D. (1993) *J. Am. Chem. Soc. 115*, 3352−3353.
9. Imperiali, B., and Rickert, K. W. (1995) *Proc. Natl. Acad. Sci. U.S.A. 92*, 97−101.
10. Inazu, T., and Kobayashi, K. (1993) *Synlett* 869−870.
11. Inazu, T., Mizuno, M., Kohda, Y., Kobayashi, K., and Yaginuma, H. (1996) in *Peptide Chemistry 1995* (Nishi, N., Ed.) pp 61−64, Protein Research Foundation, Osaka, Japan.
12. Haneda, K., Inazu, T., Yamamoto, K., Kumagai, H., Nakahara, Y., and Kobata, A. (1996) *Carbohydr. Res. 292*, 61−70.
13. Mizuno, M., Muramoto, I., Kawakami, T., Seike, M., Aimoto, S., Haneda, K., and Inazu, T. (1998) *Tetrahedron Lett. 39*, 55−58.
14. Haneda, K., Inazu, T., Mizuno, M., Iguchi, R., Yamamoto, K., Kumagai, H., Aimoto, S., Suzuki, H., and Noda, T. (1998) *Bioorg. Med. Chem. Lett. 8*, 1303−1306.
15. Yamamoto, K., Haneda, K., Iguchi, R., Inazu, T., Mizuno, M., Takegawa, K., Kondo, A., and Kato, I. (1999) *J. Biosci. Bioeng. 87*, 175−179.
16. Mizuno, M., Haneda, K., Iguchi, R., Muramoto, I., Kawakami, T., Aimoto, S., Yamamoto, K., and Inazu, T. (1999) *J. Am. Chem. Soc. 121*, 284−290.
17. Motta, A., Antonietta, M., Morelli, C., Goud, N., and Temussi, P. A. (1989) *Biochemistry 28*, 7996−8002.
18. Meadows, R. P., Nikonowicz, E. P., Jones, C. R., Bastian, J. W., and Gorenstein, D. G. (1991) *Biochemistry 30*, 1247−1254.
19. Motta, A., Temussi, P. A., Wünsch, E., and Bovermann, G. (1991) *Biochemistry 30*, 2364−2371.

20. Motta, A., Pastore, A., Goud, N. A., and Morelli, M. A. C. (1991) *Biochemistry 30*, 10444−10450.
21. Ogawa, K., Nishimura, S., Doi, M., Kyogoku, Y., Hayashi, M., and Kobayashi, Y. (1994) *Eur. J. Biochem. 222*, 659−666.
22. Motta, A., Andreotti, G., Amondeo, P., Strazzullo, G., and Morelli, M. A. C. (1998) *Proteins 32*, 314−323.
23. Epand, R. M., Epand, R. F., Orlowski, R. C., Schlueter, R. J., Boni, L. T., and Hui, S. W. (1983) *Biochemistry 22*, 5074−5084.
24. Epand, R. M., and Epand, R. F. (1986) *Biochemistry 25*, 1964−1968.
25. Murad, F., Brewer, H. B., and Vaughan, M. (1970) *Proc. Natl. Acad. Sci. U.S.A. 65*, 446−453.
26. Lin, H. Y., Harris, T. L., Flannery, M. S., Aruffo, A., Kaji, E. H., Gorn, A., Kolakowski, L. F., Lodish, H. F., and Goldring, S. R. (1991) *Science 254*, 1022−1026.
27. Opella, S. J. (1997) *Nature Struct. Biol., NMR Suppl. 4*, 845−848.
28. Cross, T. A., and Opella, S. J. (1994) *Curr. Opin. Struct. Biol. 4*, 574−581.
29. Marassi, F. M., and Opella, S. J (1998) *Curr. Opin. Struct. Biol. 8*, 640−648.
30. Marassi, F. M., Ramamoorthy, A., and Opella, S. J. (1997) *Proc. Natl. Acad. Sci. U.S.A. 94*, 8551−8556.
31. Kim, Y., Valentine, K., Opella, S. J., Schendel, S. L., and Cramer, W. A. (1998) *Protein Sci. 7*, 342−348.
32. Opella, S. J., Marassi, F. M., Gesell, J., Valente, A. P., Kim, Y., Oblatt-Montal, M., and Montal, M. (1999) *Nature Struct. Biol. 6*, 374−379.
33. Wu, C. H., Ramamoorthy, A., and Opella, S. J. (1994) *J. Magn. Reson., Ser. A 109*, 270−272.
34. Wüthrich, K. (1986) *NMR of Proteins and Nucleic Acids*, J. Wiley & Sons, New York.
35. Harbison, G. S., Jelinski, L. W., Stark, R. E., Torchia, D. A., Herzfeld, J., and Griffin, R. G. (1984) *J. Magn. Reson. 60*, 79−82.
36. Oas, T. G., Hartzell, C. J., Dahlquist, F. W., and Drobny, G. P. (1987) *J. Am.Chem. Soc. 109*, 5962−5966.
37. Hartzell, C. J., Whitfield, M., Oas, T. G., and Drobny, G. P. (1987*) J. Am. Chem. Soc. 109*, 5966−5969.
38. Teng, Q., and Cross, T. A. (1989) *J. Magn. Reson. 85*, 439−447.
39. Mer, G., Hietter, H., and Lefèvre, J. F. (1996) *Nature Struct. Biol. 3*, 45−53.
40. Wyss, D. F., Choi, J. S., Li., J., Knoppers, M. H., Willis, K. J., Arulanandam, A. R. N., Smolyar, A., Reinhertz, E. L., and Wagner, G. (1995) *Science 269*, 1273−1277.
41. O'Neil, J. D. J., and Sykes, B. D. (1989) *Biochemistry 28*, 699−707.

BI983018J